

THESIS FOR THE DEGREE OF LICENTIATE OF ENGINEERING IN THERMO  
AND FLUID DYNAMICS

Simulation and Analysis of a Novel Open Rotor Propeller -  
the Boxprop

ALEXANDRE CAPITAO PATRAO

Department of Applied Mechanics  
*Division of Fluid Dynamics*  
CHALMERS UNIVERSITY OF TECHNOLOGY  
Gothenburg, Sweden 2016

Simulation and Analysis of a Novel Open Rotor Propeller - the Boxprop  
ALEXANDRE CAPITAO PATRAO

© ALEXANDRE CAPITAO PATRAO, 2016

Thesis for the degree of Licentiate of Engineering 2016:17

ISSN 1652-8565

Department of Applied Mechanics

Division of Fluid Dynamics

Chalmers University of Technology

SE-412 96 Gothenburg

Sweden

Telephone: +46 (0)31-772 1000

Chalmers Reproservice  
Gothenburg, Sweden 2016

Simulation and Analysis of a Novel Open Rotor Propeller - the Boxprop  
Thesis for the degree of Licentiate of Engineering in Thermo and Fluid Dynamics  
ALEXANDRE CAPITAO PATRAO  
Department of Applied Mechanics  
Division of Fluid Dynamics  
Chalmers University of Technology

## ABSTRACT

Economic factors and environmental awareness is driving the evolution of aircraft engines towards increasingly higher efficiencies, reaching for lower fuel consumption and lower emissions. The Counter-Rotating Open Rotor (CROR) is actively being researched around the world, promising a significantly increased propulsion efficiency relative to existing turbofans by employing two, counter-rotating propeller blade rows, thereby increasing the bypass ratio of the engine. Historically, these engines have been plagued by very high noise levels, mainly due to the impingement of the front rotor tip vortices on the rear rotor. In modern designs, the noise levels have been significantly decreased by clipping the rear, counter-rotating propeller. Unfortunately, this comes at a cost of decreased efficiency.

An alternative, potential solution lies with the Boxprop, which was invented by Richard Avellán and Anders Lundbladh. The Boxprop consist of blade pairs joined at the tip, and are conceptually similar to box wings. It is hypothesized that the Boxprop can eliminate the tip vortex found in conventional blades, consequently increasing the efficiency of the blades, and reducing their acoustic signature.

The present work highlights advances done in the research surrounding the Boxprop. A validation of the deployed CFD methodology is presented, in which numerical and experimental results compare favourably. Performance results for a Boxprop (GP-X-701) designed for cruise conditions are presented and compared with a generic conventional propeller (GP-S-609). It is shown that the present Boxprop cruise design can reach the required thrust for replacing the front rotor of a modern CROR, but with increased swirl relative to the analyzed conventional propeller. This is mainly due to the effect of the blade passage unloading one of the Boxprop blade halves near the tip, forcing the blade to be more highly loaded closer to the hub. The swirl generated by the Boxprop could be partially recovered if it is used together with a rear counter-rotating propeller.

A Wake Analysis Method (WAM) is presented in this work and is used to quantify the power flows inherent to the flow features of the propeller wake. The power flows can be characterized as propulsively beneficial, recoverable, or pure losses. It has the ability to distinguish the kinetic energies of the tip vortices, wakes, and other disturbances from the flow field.

The Wake Analysis Method was applied on the two propellers mentioned earlier, and confirmed that the Boxprop produces 50% more swirl than the conventional propeller. Additionally, the method very clearly shows the lack of tip vortex on the Boxprop, and the presence of it in the flow field of the conventional propeller.

Keywords: Open Rotors, Propfans, Propellers, CROR, CFD, Tip vortex, Wake Analysis Method



## LIST OF PUBLICATIONS

This thesis is based on the work contained in the following publications:

- I R. Avellán, A. Capitaó Patrao, A. Lundbladh, and T. Grönstedt, 2015, Preparing for Proof-of-Concept of a Novel Propeller for Open Rotor Engines, *22nd ISABE Conference*, October 25–30, Phoenix, USA
- II A. Capitaó Patrao, R. Avellán, A. Lundbladh, and T. Grönstedt, 2016, Wake and Loss Analysis for a Double Bladed Swept Propeller, *Proceedings of ASME Turbo Expo 2016*, June 13–17, Seoul, South Korea



## ACKNOWLEDGEMENTS

This work would have been significantly more challenging without the support from my supervisor Tomas Grönstedt, whose advice and counsel has been of great help, both when facing *seemingly* insurmountable obstacles and in better times. I am very grateful that I have been given the opportunity to work with something this interesting and enjoyable.

I would like to extend my gratitude to Anders Lundbladh and Richard Avellán at GKN Aerospace for their continuing advice and feedback in all areas related to aerospace. Their encyclopedic knowledge in that area has been of great help during the project, and for an aviation nut as myself, our discussions (especially at airports) have been thoroughly enjoyable!

To my present and past colleagues at Chalmers, thanks for creating a great and inspiring working environment. Special thanks to my roomie Marcus Lejon for being a very good friend and colleague. I always enjoy our talks, whether it is about compressors, propellers, or if something can be made into a smoothie or not. Thanks to my previous roomie Basti for introducing and guiding me at the department when I first started my time as a PhD student.

Master thesis students Isak Jonsson, Sandra Busch, and Gonzalo Montero Villar - thank you for your contribution to the research and your great company, I learned a great deal from you!

Finally, I would like to thank my family and my wonderful girlfriend for their enduring support and belief in me, I would not have gotten anywhere without them.

This research was funded by the Swedish National Aviation Engineering Research Programme, NFFP. The author would like to acknowledge the financial support of VINNOVA, the Swedish Defence Material Administration (FMV) and GKN Aerospace. Additionally, the author would like to extend his gratitude to the Chalmers Centre for Computational Science and Engineering (C3SE), Gothenburg, Sweden, for providing support and the necessary computational infrastructure for the research.





*When eating an elephant take one bite at a time.*  
- Creighton Abrams.



# NOMENCLATURE

## Roman upper case letters

$A$	Integration area for the Wake Analysis Method [ $m^2$ ]
$B$	Number of blades
$C_P$	Coefficient of power
$C_T$	Coefficient of thrust
$D$	Propeller tip diameter [ $m$ ]
$D'$	Sectional drag [ $N/m$ ]
$J$	Advance ratio
$L$	Lift [ $N$ ]
$L'$	Sectional lift [ $N/m$ ]
$P_{shaft}$	Shaft power [ $W$ ]
$R$	Tip radius [ $m$ ]
$T$	Thrust [ $N$ ]
$T'$	Sectional thrust [ $N/m$ ]
$U_i$	Circumferentially averaged velocity component [ $m/s$ ]
$V$	Velocity magnitude [ $m/s$ ]
$\dot{W}$	Work done on the fluid per unit time [ $W$ ]

## Roman lower case letters

$c$	Chord [ $m$ ]
$h$	Static specific enthalpy [ $J/kg$ ]
$h_0$	Total specific enthalpy [ $J/kg$ ]
$k$	Turbulent kinetic energy [ $J/kg$ ]
$\dot{m}$	Mass flow [ $kg/s$ ]
$n$	Revolutions per second [ $1/s$ ]
$r$	Radius [ $m$ ]
$t$	Airfoil profile thickness [ $m$ ]
$u_i$	Velocity component $i$ [ $m/s$ ]
$v_i$	Velocity perturbation component [ $m/s$ ]

## Greek letters

$\alpha$	Angle-of-attack [ $^\circ$ ]
$\Gamma_{wake}$	Wake circulation [ $m^2/s$ ]
$\Delta$	Change in variable value
$\epsilon$	Drag-to-lift ratio
$\eta_{prop}$	Propeller efficiency
$\xi$	Normalized radial position
$\rho$	Density [ $kg/m^3$ ]
$\phi$	Flow angle [ $^\circ$ ]

## Subscripts

1	Inlet conditions
2	Wake Analysis plane conditions
$\infty$	Freestream conditions
$n$	Normal direction
$r$	Relative frame
$x$	Axial direction
$\theta$	Tangential direction

## Abbreviations

<i>AF</i>	Activity Factor
<i>BB</i>	BoxBlade
<i>CAD</i>	Computer Aided Design
<i>CB</i>	Conventional Blade
<i>CFD</i>	Computational Fluid Dynamics
<i>CROR</i>	Counter-Rotating Open Rotor
<i>DDR</i>	Dual rotor Dynamic test Rig
<i>EBM</i>	Electron Beam Melting
<i>FEM</i>	Finite Element Method
<i>HTR</i>	Hub-to-Tip Ratio
<i>ICAO</i>	International Civil Aviation Organization
<i>LB</i>	Leading Blade
<i>R&amp;D</i>	Research and Development
<i>SLM</i>	Selective Laser Melting
<i>SSR</i>	Single rotor Static Rig
<i>SST</i>	Shear Stress Transport
<i>TB</i>	Trailing Blade
<i>WAM</i>	Wake Analysis Method

# CONTENTS

<b>Abstract</b>	<b>i</b>
<b>List of publications</b>	<b>iii</b>
<b>Acknowledgements</b>	<b>v</b>
<b>Nomenclature</b>	<b>ix</b>
<b>Contents</b>	<b>xi</b>
<b>1 Introduction</b>	<b>1</b>
<b>2 The Boxprop</b>	<b>3</b>
2.1 Boxprop description . . . . .	3
2.2 Hypotheses . . . . .	4
2.3 Propeller performance parameters . . . . .	5
2.4 Previous work on the Boxprop . . . . .	6
2.5 Design evolution of the Boxprop . . . . .	6
<b>3 Wake Analysis Method</b>	<b>9</b>
3.1 Derivation . . . . .	9
<b>4 Propeller designs</b>	<b>12</b>
4.1 GP-X-313 . . . . .	12
4.2 GP-X-701 . . . . .	13
4.3 GP-S-609 . . . . .	14
<b>5 CFD methodology</b>	<b>15</b>
5.1 Flow modelling . . . . .	15
5.2 Meshing for performance . . . . .	16
5.3 Meshing for the Wake Analysis Method . . . . .	17
<b>6 Results</b>	<b>18</b>
6.1 Experimental validation of CFD methodology . . . . .	18
6.2 Cruise performance results . . . . .	19
6.3 Wake Analysis results . . . . .	23
6.4 Boxprop tip flow . . . . .	27
<b>7 Conclusions</b>	<b>28</b>
7.1 Meshing . . . . .	28
7.2 Performance and modelling . . . . .	28
<b>8 Future work</b>	<b>29</b>

**9 Summary of Papers** **30**

9.1 Paper I . . . . . 30

9.1.1 Division of work . . . . . 30

9.1.2 Summary . . . . . 30

9.2 Paper II . . . . . 31

9.2.1 Division of work . . . . . 31

9.2.2 Summary . . . . . 31

# 1 Introduction

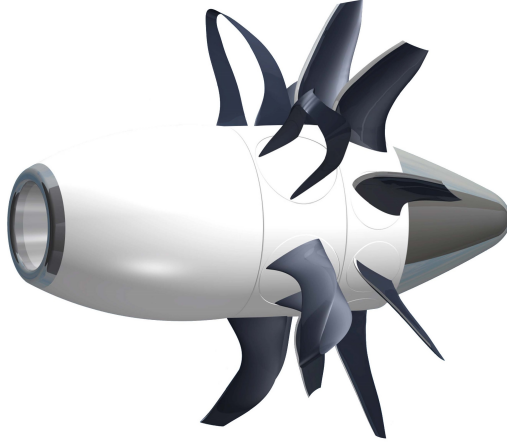


**Figure 1.0.1:** *Illustration of a pusher-type Counter-Rotating Open Rotor (CROR) concept using Boxprop blades. Image credit: [1].*

A major focus of the R&D activities of transport industries in the world regards the reduction of fuel consumption. The major benefits lie in decreased cost, lower greenhouse gas emissions, and improved public health. More fuel-efficient transportation is a challenge shared across several major modes of transport, including automotive, naval, and aviation.

In aviation, the amount of passengers is estimated to have reached 3.5 billion yearly passengers in 2015, and is expected to reach an astounding 7 billion by 2034, averaging a yearly growth rate of 3.8% [2]. In this particular industry, fuel has always been a considerable contributor to the costs of operating aircraft, accounting for 29% of all airline costs in 2015 [3]. In terms of greenhouse emissions, the aviation industry emits an estimated 2% of the global anthropogenic  $CO_2$  emissions [3]. Additionally, the  $NO_x$  emissions from jet engines have detrimental effects on the environment (acid rain) and on public health, possibly causing or worsening certain types of respiratory diseases [4].

In contrast to the current level and projected growth of air travel, the aviation industry as a whole has agreed on halving the emissions by 2050 (compared to 2005) [2], a goal to strive for by improving all aspects of aviation operations. Aero engines will have to play its part by introducing new innovative technologies and concepts. These new technologies can include new heat recuperation concepts, unconventional combustion technologies, and novel propulsive systems [5]. More integrated powerplant and aircraft configurations may also pave a way forward [6].

Counter-Rotating Open Rotors (CROR) which are part of the aforementioned technologies, offer potential fuel savings in the range of 20-35% [7], and are being actively researched around the world ([8], [9], [10]). Flight demonstrations were performed by the US in the 1980's and Europe is gearing up for flight demonstrations in the 2020's [11].

One of the major issues concerning the CROR is one of noise, which is due to the tip vortices and wakes from the front propeller blades impinging on the rear propeller blades. The noise level is one of several hurdles in the way to commercial adaptation of the CROR, and the noise level has to be decreased below current and future ICAO noise standards in order for it to be widely adapted in the aviation industry.

The Boxprop concept (illustrated in Figure 1.0.1) was conceived by Richard Avellán and Anders Lundbladh in 2009, drawing inspiration from Prandtl's theory on wings with minimum induced drag. The Boxprop consists of pair-wise tip-joined blades, conceptually similar to box wings. The shape of the blades can potentially reduce the tip vortex strength, leading to higher efficiency and lower interaction noise, and incorporate higher structural rigidity. If the Boxprop is used as a front rotor of a CROR, then the increased rigidity can allow forward sweep, increasing the distance between each counter-rotating rotor. This increased distance allows more mixing of the tip vortices and wakes, which is also beneficial from a noise perspective.

The Boxprop has an interesting mix of potentially valuable properties and challenges in its design. This thesis seeks to convey some of the work that has been done on the Boxprop, both numerical and experimental, in order to further the understanding of its performance, flow physics, and potential benefits.



# 2 The Boxprop

This section will briefly describe the Boxprop concept and its geometry, main hypotheses, propeller performance parameters, and previous work done on the Boxprop. The section will end with brief note on the evolution of the Boxprop design.

## 2.1 Boxprop description

The Boxprop draws inspiration from non-planar wings (see Figure 2.1.1), variations of which have been used historically in the form of biplanes (and triplanes). More recently, non-planar wings are found on wings of modern aircraft in the form of wingtip devices such as winglets and sharklets. Kroo [12] calculated the induced drag coefficient of several types of non-planar wings relative to a planar wing, and the results have been reproduced in Figure 2.1.1. As was shown by Kroo, for the same span and lift, the boxwing produces significantly less induced drag than the conventional planar wing. It can also be seen that planar wings with winglets offer a substantial efficiency gain, which partially explains their prevalence on modern aircraft designs with smaller aspect ratio wings. The various wing shapes in Figure 2.1.1 all weaken the tip vortices and their associated losses.

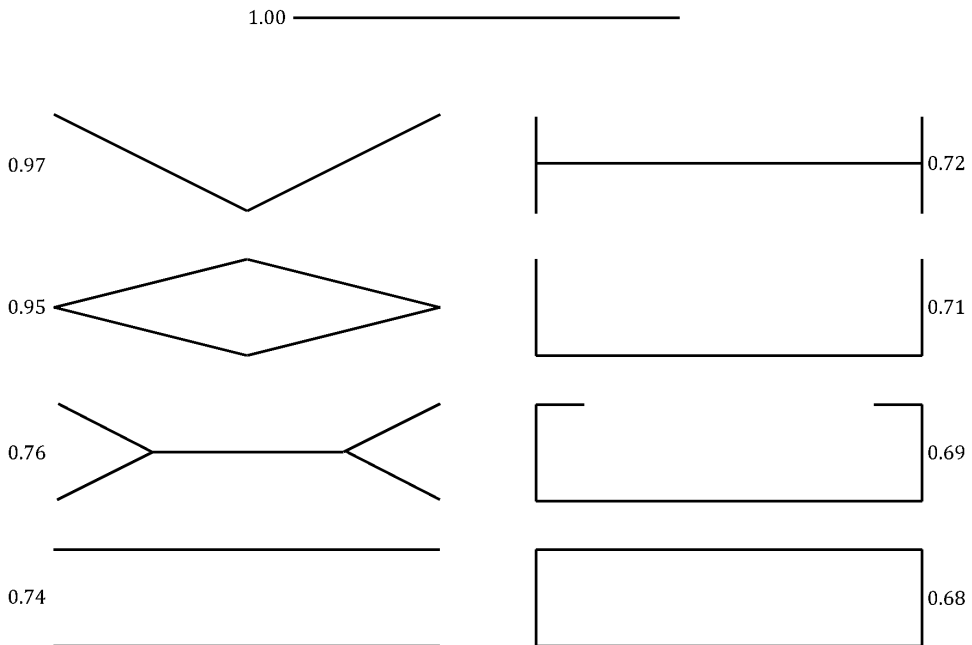


**Figure 2.1.1:** Non planar wing concepts and their induced drag relative to a planar wing of the same span and lift. The box wing exhibits the lowest induced drag of all presented concepts. Adapted from: [12]

The fundamental function of propellers is similar to wings, and therefore the concept of non-planar wings was transformed by Richard Avellán & Anders Lundbladh [13] into the Boxprop by joining two propeller blades at the tips, as seen in Figure 2.1.2. The two blade halves are denoted *Leading Blade (LB)* and *Trailing blade (TB)* with respect to the rotational direction. The blade geometry is constructed using an in-house code called BBCode [14], which constructs an arc-shaped stacking line, and stacks airfoil sections along its length. The airfoil sections are of the NACA 16 type [15], and chord, thickness, camber, and angle-of-attack distributions are used to construct and properly position the airfoils on any given position along the stacking line. Sweep, lean and blade geometrical separation is controlled with the parametrization of the stacking line. Extensive documentation on BBCode can be found in the theses by Adriansson [14] and by Olofsson & Pettersson [16].

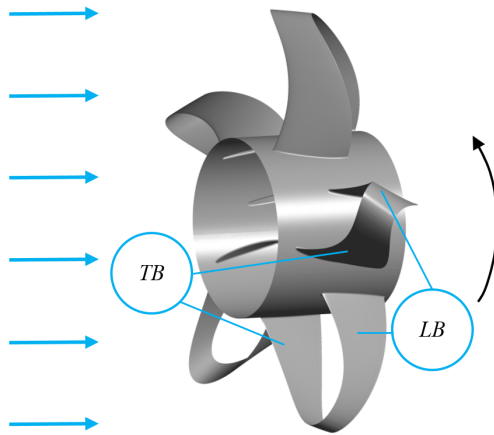


**Figure 2.1.2:** *Boxprop* blade notation, direction of rotation and inflow direction.

## 2.2 Hypotheses

As was mentioned briefly in the Introduction, there are two main hypotheses regarding the Boxprop:

- The tip joined blades will suppress the tip vortex, leading to lower induced drag. A non-suppressed tip vortex will impinge on the rear rotor of a CROR, increasing noise. See Figure 3 for illustration. Modern CROR designs solve this issue by clipping the rear propeller, allowing the front rotor tip vortex to pass by without impinging on the rear rotor. It is worth remembering that rear rotor clipping is a compromise – clipping the blade can yield lower propeller efficiency at cruise conditions [7].
- Higher structural rigidity allows forward sweep with less risk for flutter. As can be seen in Figure 3, the forward sweep increases the axial spacing between front and rear propellers in a CROR setup, resulting in a longer travel path for the tip vortices

(if present) and wakes, weakening these perturbations and potentially decreasing their acoustic impact. Increasing axial spacing can also be achieved by translating the blades in the axial direction, but this unfortunately also results in increased engine weight [7].

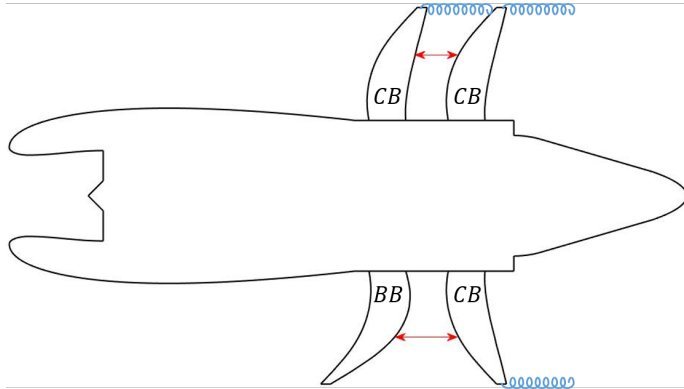


**Figure 2.2.1:** The **upper half** of the image illustrates a generic CROR with conventional back-swept blades (CB). Tip vortices are created in the tips of each blade. The tip vortices and wakes of the front blade impinge on the rear blade, creating high levels of noise. The **lower half** of the image depicts a CROR using a front-swept boxblade (BB) as the front rotor, and a conventional blade (CB) as the rear rotor. The axial spacing ( $\leftrightarrow$ ) between the rotors at  $0.75R$  is illustrated for both configurations, and shows that the forward swept blade achieves a larger spacing for equivalent sweep and chord distributions.

## 2.3 Propeller performance parameters

Propeller performance is typically specified in terms of non-dimensional numbers. These include the advance ratio  $J$ , power coefficient  $C_P$ , thrust coefficient  $C_T$ , and propeller efficiency  $\eta_{prop}$ , as defined in Eq. 2.3.1 to 2.3.4.

$$J = \frac{V_\infty}{nD} \quad (2.3.1)$$

$$C_P = \frac{P_{shaft}}{\rho_\infty n^3 D^5} \quad (2.3.2)$$

$$C_T = \frac{T}{\rho_\infty n^2 D^4} \quad (2.3.3)$$

$$\eta_{prop} = \frac{TV_\infty}{P_{shaft}} \quad (2.3.4)$$

The *Activity Factor*  $AF$  is a measure of the propeller area, and a larger  $AF$  results in a propeller that can absorb more power:

$$AF = \frac{10^5}{16} \int_{\xi_{hub}}^{\xi_{tip}} \left(\frac{c}{D}\right) \xi^3 d\xi \quad (2.3.5)$$

The chord is weighted by the non-dimensional radius  $\xi$  cubed, meaning that a propeller with a specific chord at the tip can input more power than one with the same chord near the hub.

## 2.4 Previous work on the Boxprop

A number of Master Thesis projects were performed before the start of the work described in this thesis. The authors and their respective contributions will be briefly mentioned in this section:

- **Adriansson** - Wrote the first version of the in-house code *BBCode*, which can be used for blade geometry creation, preliminary performance assessment, and output to CAD software.
- **Carlsvärd** - Constructed and designed the first Boxprop testing rig, the *Single rotor Static test Rig* (SSR), and designed an additional rig for counter-rotating propellers, the *Dual rotor Dynamic test Rig* (DDR).
- **Lind** - Performed CFD calculations to obtain performance data on early small scale Boxprop designs at take-off and cruise conditions.
- **Olofsson & Pettersson** - Carried out rapid prototype manufacturing and testing of small scale Boxprops. To support this, work was continued on the DDR rig designed by Carlsvärd, *BBCode* was extended, and FEM-analyses were performed, resulting in new Boxprop designs with improved thrust and efficiency.

## 2.5 Design evolution of the Boxprop

The design point chosen for the Boxprop is set to an altitude of 10 668 *m* and a cruise Mach number of 0.75, which is representative for a future passenger aircraft equipped with open rotor engines ([7],[17]). Initially during the research project the cruise Mach number was set to 0.7, largely in part due to the availability of results and data from previous research projects regarding the Boxprop. This data facilitated the initial Boxprop design changes and was of great help increasing its performance.

The Boxprop design has gone through a number of geometric changes in order to reach higher efficiency and performance, the effects of which are illustrated in Figure 2.5.1. The main drivers of the performance increase lie in: (A) a better adapted blade tip to the slipstream tube, (B) changing the blade section angle-of-attack and blade passage spacing,

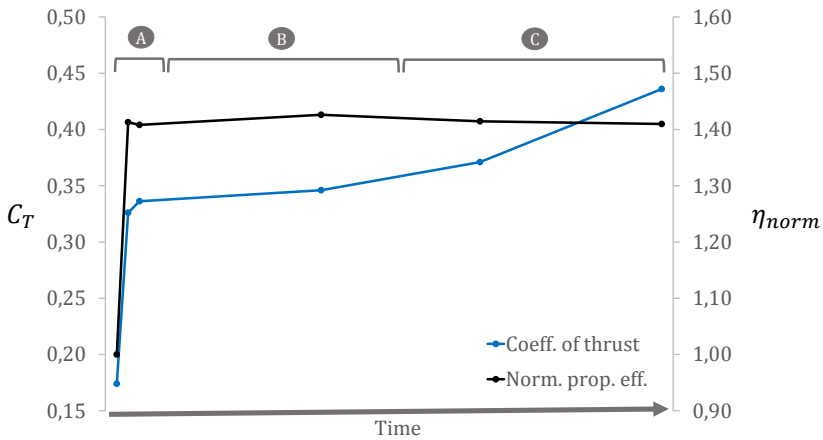


**Figure 2.5.1:** *Bozprop* performance development over time in terms of coefficient of thrust and normalized propeller efficiency.

and (C) tailoring the angle-of-attack and camber distributions for each blade half. This tailoring is required to account for the induced flow each blade half has on each other and to decrease the blade interference.

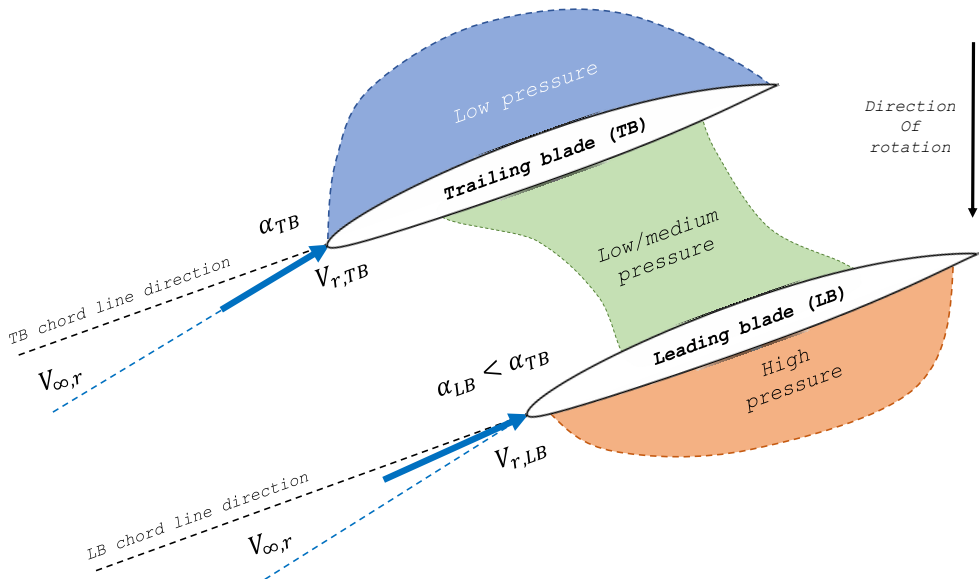


**Figure 2.5.2:** Illustration of the encountered blade interference phenomena in a two-dimensional cut of the Bozblade. The blue arrows denote the relative flow velocities, and as can be seen, the LB incidence is affected by the flow from the TB, leading to lower loading. Also visible is the low/medium pressure region that can form in the blade passage.

The aforementioned blade interference includes two main phenomena and is illustrated in Figure 2.5.2. The *first* phenomenon is a decrease in loading of the LB due to the induced flow from the TB, which effectively lowers the angle-of-attack of the LB, and decreases its sectional lift and thrust. For the LB to deliver similar sectional thrust as the TB, its angle-of-attack has to be increased by changing the blade angle. The *second* observed phenomenon is the low pressure region that forms in the passage between the blade halves. This region forms whenever the placement of the airfoils, their camber, and their thickness create a contracting passage between the blades, and it effectively unloads the TB by hindering the creation of the high pressure that would otherwise be created on the TB pressure side. If the passage cross-sectional area decreases aggressively, choking might also occur. Consequently, in order to load the TB properly its camber or the blade spacing can be increased (this will unfortunately also off-load the LB). Alternatively, the blade angle of the LB can be increased and its camber decreased, thereby increasing the distance to the TB. In conclusion, both these measures decrease the contraction in the blade passage.

# 3 Wake Analysis Method

The *Wake Analysis Method* (WAM) was developed in order to quantify the wake structures found in Boxprops and conventional propellers in terms of engine power, allowing different types of propellers to be analyzed and their losses compared on equal terms. In general, the method is applied on a surface downstream of the propeller (or any type of rotor) and relates the properties on that plane to the inflow properties.

## 3.1 Derivation

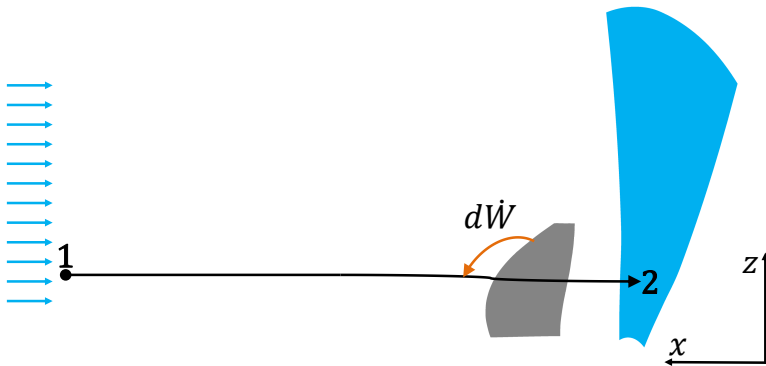


**Figure 3.1.1:** Illustration of the work per unit time added to a fluid element flowing from a point far upstream (1) to a point downstream of the propeller (2). A slice of the area of integration for one blade passage is marked blue behind the propeller blade.

The WAM relates the energy changes in particles that travel through a generic rotor (this case a propeller), and enables a breakdown of these energies into enthalpy, kinetic, and turbulent kinetic energy. Consider an elemental fluid element flowing through a turbomachine, as shown in Figure 3.1.1. In a coordinate system rotating with the rotor, the flow can be considered to be steady. However, the velocities will be defined in reference to a stationary frame. The work per unit time added to the particle between a point upstream of the rotor and a control point downstream of the rotor lying on a plane, can be calculated from the total enthalpy change  $\Delta h_0$ , as specified in Eq. 3.1.1, where  $u_n$  is the velocity normal to the plane. For the case of the propeller, the plane lies parallel to the  $yz$ -coordinate plane, and the normal velocity becomes the axial velocity.

$$d\dot{W} = \Delta h_0 d\dot{m} = \Delta h_0 \rho_2 u_n dA \quad (3.1.1)$$

In order to account for all the power transferred from the propeller ( $P_{shaft}$ ) to the fluid, the particle work per unit time is integrated over an annular area  $A$  behind the propeller:

$$P_{shaft} = \int_A d\dot{W} = \int_A \Delta h_0 \rho_2 u_n dA \quad (3.1.2)$$

The slice of area  $A$  corresponding to one propeller blade passage is shown in Figure 3.1.1. The total enthalpy change can be expanded into its constituents according to:

$$\Delta h_0 = \Delta \left( h + \frac{1}{2} u_i u_i + k \right) \quad (3.1.3)$$

Where  $u_i$  is the time-averaged velocity in direction  $i$ . The change in total enthalpy is calculated as the difference between the points on the plane behind the propeller and far upstream, per Eq. 3.1.4.

$$\Delta h_0 = h_{0,1} - h_{0,2} \quad (3.1.4)$$

The kinetic energy can be further expanded into its components, using a cylindrical coordinate system:

$$\frac{1}{2} u_i u_i = \frac{1}{2} (u_x^2 + u_r^2 + u_\theta^2) \quad (3.1.5)$$

Equations 3.1.2 to 3.1.5 yield the split of the input power into the integral of the flow variables in the wake:

$$P_{shaft} = \int_A \rho_2 u_n \left[ (h_2 - h_1) + \frac{1}{2} (u_{x,2}^2 - u_{x,1}^2) + \frac{1}{2} (u_{r,2}^2 - u_{r,1}^2) + \frac{1}{2} (u_{\theta,2}^2 - u_{\theta,1}^2) + (k_2 - k_1) \right] dA \quad (3.1.6)$$

In order to capture the structure of the wake and tip vortex, the velocities  $u_i(r, \theta)$  can be decomposed into a *circumferentially averaged velocity*  $U_i(r)$  and an associated *perturbation*  $v_i(r, \theta)$ :

$$u_i(r, \theta) = U_i(r) + v_i(r, \theta) \quad (3.1.7)$$

$$U_i = \frac{1}{\kappa} \int_0^{2\pi} \rho_2 u_n u_i d\theta \quad \kappa = \int_0^{2\pi} \rho_2 u_n d\theta \quad (3.1.8)$$

The flow is assumed to be purely axial and uniform far upstream of the propeller, and applying Eq. 3.1.5 to the terms of the integrand in Eq. 3.1.6 results in the following expression for the kinetic energies:

$$u_{x,2}^2 - u_{x,1}^2 = (U_{x,2}^2 - U_{x,1}^2) + v_{x,2}^2 \quad (3.1.9)$$

$$u_{r,2}^2 - u_{r,1}^2 = U_{r,2}^2 + v_{r,2}^2 \quad (3.1.10)$$

$$u_{\theta,2}^2 - u_{\theta,1}^2 = U_{\theta,2}^2 + v_{\theta,2}^2 \quad (3.1.11)$$

The cross-terms (e.g.  $2U_{x,2}v_{x,2}$ ) that would appear in Eq. 3.1.9 to 3.1.11 become zero when integrated in Eq. 3.1.6 and are therefore neglected.

The perturbation terms constitute the velocity variation behind each blade of the propeller and do not carry any mean axial momentum, and therefore do not contribute to



thrust. For a highly loaded propeller most of the energy in these terms are associated with the tip vortices and wakes of the blades.

For propellers, an increase in static enthalpy ( $h_2 - h_1$ ) can be due to an increase in pressure through the propeller plane as is described by the *Actuator Disc Theory*, or due to dissipation of kinetic energy or turbulent kinetic energy. A decrease in static enthalpy can be due to a decrease in pressure, which occurs downstream of the propeller disc, where it is converted into axial kinetic energy. The turbulent kinetic energy increase occurs mainly in the boundary and shear layers present in the flow, which for a propeller corresponds to the wetted surfaces, wakes, and tip vortices.

# 4 Propeller designs


Worth mentioning in this thesis are three particular propeller designs:

- **GP-X-313** - Used for validation of the CFD methodology using experiments performed in the Chalmers Wind Tunnel.
- **GP-X-701** - Designed to deliver high thrust at cruise and analysed with the WAM.
- **GP-S-609** - Generic conventional propeller inspired by the NASA SR-7L high speed propeller [18]. Analysed with the WAM and compared to the GP-X-701.

## 4.1 GP-X-313

The GP-X-313 was originally designed by Olofsson and Pettersson [16], and has been extensively analysed, both numerically and experimentally. This propeller has served as an experimental validation case for the CFD methodology, and the performance results are shown in Chapter 6. The propeller design is specified in Figure 4.1.1. This particular propeller is scaled down to do a diameter of  $150\text{ mm}$ , enabling it to be run in the Chalmers Wind Tunnel. The blade thickness is relatively high compared to propellers designed for cruise, but the high thickness was a requirement for the chosen manufacturing process (3D-printed plastic). This propeller also features a blade tip modification that the cruise propellers do not. The slipstream of propellers operating at low axial velocities usually contracts, which has led to this propeller having an *inflow cone angle* of  $13^\circ$ . This cone angle essentially means that the tip of the blade is re-pitched to match the slipstream shape.

<b>GP-X-313</b>	
$B$	5
$D$	$0.15\text{ [m]}$
$HTR$	0.4
$AF$	1800
<i>Airfoil profile</i>	NACA 16
$(t/c)_{hub}$	14%
$(t/c)_{tip}$	7%
<i>Inflow cone angle</i>	$13^\circ$



**Figure 4.1.1:** *GP-X-313 propeller specification and shape.*

## 4.2 GP-X-701

This propeller is the end result of the Boxprop design evolution described in Section 2.5, and was designed for cruise conditions, which corresponds to an axial Mach number of 0.75 and a cruise altitude of 10 668  $m$ . The goal of this propeller was to obtain a thrust coefficient  $C_T$  comparable to what is found in published CROR front rotor designs ([7], [17]).

The diameter of this propeller has been increased somewhat relative to the GP-X-313, enabling higher Reynolds numbers and performance more similar to full-scale propellers. The profile thickness has been decreased markedly relative to the GP-X-313, since this propeller operates at cruise conditions and was not run in any experiments. Consequently, the manufacturing limitations associated with 3D-printing can be ignored. The blade tip of this Boxprop design does not feature the tip modification of the GP-X-313, since it is only run at cruise conditions where the slipstream contraction is relatively small.

The blade was designed with an activity factor calculated from a modified NASA SR7L [18] propeller, which is a well-documented and frequently referenced propeller design. The modified SR7L is clipped from the bottom at 40% radius, and the resulting activity factor is then used to scale the GP-X-701 chord distribution, thus ensuring a propeller blade area equivalent to the SR7L.

<b>GP-X-701</b>	
$B$	5
$D$	0.75 [m]
$HTR$	0.4
$AF$	1784
<i>Airfoil profile</i>	NACA 16
$(t/c)_{hub}$	6.22%
$(t/c)_{tip}$	1.64%
<i>Inflow cone angle</i>	0°

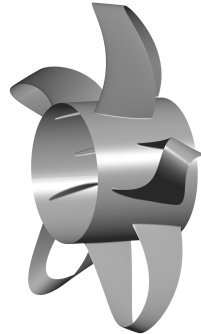


**Figure 4.2.1:** *GP-X-701 propeller specification and shape.*

### 4.3 GP-S-609

The propeller wake structures of the GP-X-701 needed to be compared to the ones of a conventional propeller. For this comparison to be more fruitful, the propellers should be analysed on an equal-thrust basis. Therefore, the GP-S-609 was designed to achieve a thrust coefficient similar to the GP-X-701.

The blade geometry is inspired by the NASA SR7L propeller [18], and uses the same airfoil profile, number of blades, chord, thickness, and camber distributions, but a different blade twist. The blade twist is different since the GP-S-609 has a different operating point than the SR7L.

<b>GP-S-609</b>	
$B$	8
$D$	0.75 [m]
$HTR$	0.4
$AF$	1784
<i>Airfoil profile</i>	NACA 16
$(t/c)_{hub}$	6.17%
$(t/c)_{tip}$	2.19%

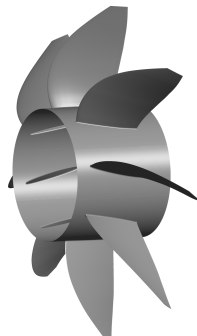


**Figure 4.3.1:** *GP-S-609 propeller specification and shape.*

# 5 CFD methodology

The types of simulations performed in this work have fallen into two discernible groups, the first being performance estimation (thrust, efficiency, etc.) and the second being a more detailed and accurate WAM. This section will mention the shared methodology used in both types of simulations.

## 5.1 Flow modelling

All CFD results presented in this thesis were obtained using ANSYS CFX, a finite-volume, implicit solver commonly used in turbomachinery applications. The governing equations are the Favre-averaged Navier-Stokes equations together with the *Shear Stress Transport* (SST) turbulence model, which is coupled with a low-Reynolds near wall formulation.

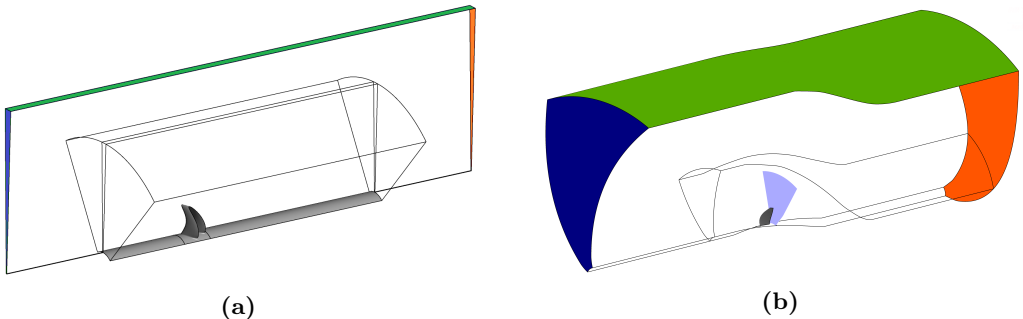


**Figure 5.1.1:** Domain setup used for (a) performance and (b) WAM simulations. The propellers are simulated using an inner, rotating domain containing the blade, and an outer, stationary domain. Blue denotes an inlet, green an opening (far field), and orange an outlet boundary condition. An example of a WAM integration plane is shown as violet in (b).

The type of domain used depends on the aims of the simulation, namely if it is for determining performance (thrust, efficiency) or if it is used for a more complex WAM, see Figure 5.1.1. Common for both cases is that the setup consists of an inner rotating domain containing the blade, and an outer stationary domain providing a far-field environment for the propeller, both connected through *Frozen Rotor* interfaces [19].

For performance calculations, the rotating inner domain containing the blade can be made smaller (even smaller than illustrated) and it does not necessarily need to follow the path of the flow. The outer, non-rotating domain reduces the flow to axisymmetric, and is there to provide a far-field environment for the inner rotating domain. For the domain setup used in simulations for the WAM, the inner domain approximately follows the orientation of the flow at each radii, aligning the mesh along the flow direction. The outer domain is no longer 2D, in order to decrease numerical error in the *Frozen Rotor* interfaces. The boundary conditions are set according to Figure 5.1.1, with more information on their specification in a thesis by Lind [20].

## 5.2 Meshing for performance

Initially, Boxprops and conventional propellers were meshed with ANSYS Meshing, which produced tetrahedral meshes everywhere in the rotating domain except at the blade and hub surfaces, whose boundary layers were discretized with triangular prism elements. This approach resulted in very low turnaround times and yielded sufficient accuracy for performance simulations. Mesh convergence studies for the Boxprop yielded differences in performance results lower than 1% for mesh sizes ranging from 5 to 30 million cells. An example of a tetrahedral mesh for a conventional blade is shown in Figure 5.2.1. The main disadvantage of this approach is a higher amount of cells when compared to a hexahedral mesh, and higher unphysical dissipation of wakes and tip vortices, making this type of mesh unsuitable for the WAM. For steady state simulations of the performance of single propellers and even counter-rotating propellers, this type of mesh is adequate, and in the latter case a mixing plane interface is added between the two counter-rotating propeller domains, which by definition mixes out the flow properties in the circumferential direction.

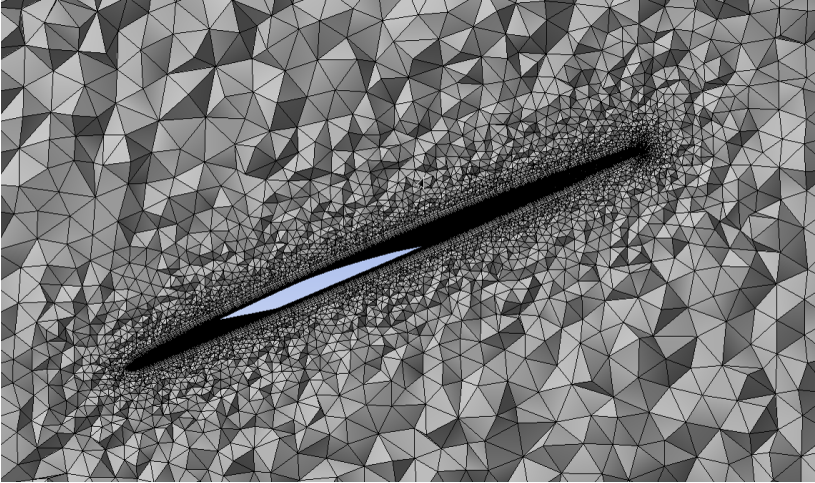


**Figure 5.2.1:** *A tetrahedral mesh for a conventional propeller. Triangular prism elements populate the boundary layer.*

### 5.3 Meshing for the Wake Analysis Method

Due to the inherent disadvantages in using tetrahedral meshes, it was decided to switch over to hexahedral meshes. They offer higher accuracy compared to tetrahedral meshes, especially if the mesh is aligned with the flow direction, as shown for a conventional propeller in Figure 5.3.1. For the WAM, the mesh needs to be fine enough to properly resolve blade wakes and tip vortices, which requires the mesh to be very fine in the directions normal to the flow direction. The mesh in Figure 5.3.1 represents the coarsest mesh used for the wake analysis of the conventional propeller presented in section 4, and contained 3.45 million cells. A mesh convergence study with respect to the terms of the WAM (specifically Eq. 3.1.6 to 3.1.11) was performed, and yielded final meshes containing 29.1 and 47 million cells for the GP-S-609 and GP-X-701, respectively. The main refinements of the mesh occurred in the mesh blocks downstream of the blade trailing edge, with some refinements in adjacent blocks.

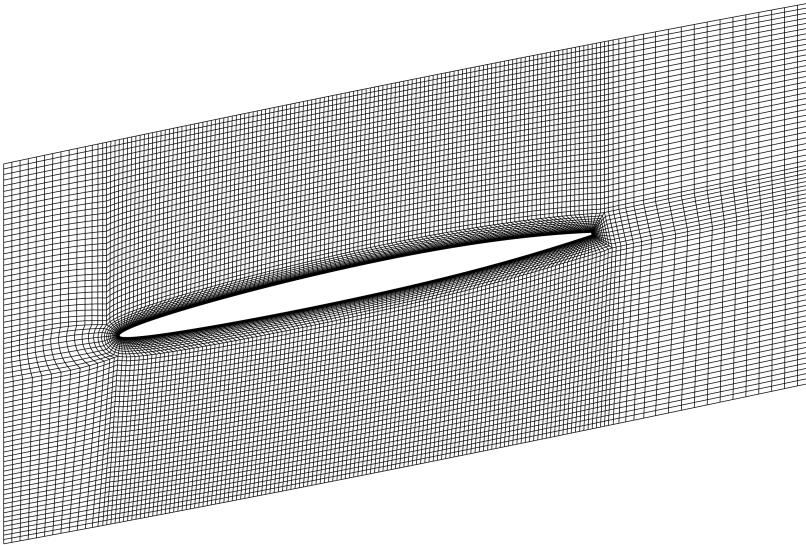


**Figure 5.3.1:** A coarse hexahedral mesh used for the WAM. Note that only a part of the domain is shown.

# 6 Results

## 6.1 Experimental validation of CFD methodology

The GP-X-313 propeller has been used as a validation case for the CFD methodology presented in Section 5. The work consisted of CFD simulations and experimental runs in the Chalmers Wind Tunnel, and was part of the Master's Thesis by Busch and Jonsson [21], and supervised by the author of this thesis.

The obtained CFD results seen in Figure 6.1.1 show very good agreement with the experimental results. The trends match and the absolute values are similar. The performance values are shown for varying advance ratio, which was adjusted by changing the freestream axial velocity and keeping the rotational velocity constant. There are two CFD cases, the first being a simulation using a propeller with a hydraulically smooth surface, a simple cylindrical hub, and no deformation due to centrifugal stresses. The second case (*compensated CFD*), includes surface roughness, the real nacelle geometry used in experiments and blade deformation.

The similarity of the computational and experimental data for the GP-X-313 increases the confidence of the adopted CFD methodology. Unfortunately, the Chalmers Wind Tunnel cannot achieve high enough axial Mach numbers for validation of the CFD simulations at cruise conditions. Nevertheless, this work shows very good agreement between experiments and CFD at near take-off conditions.

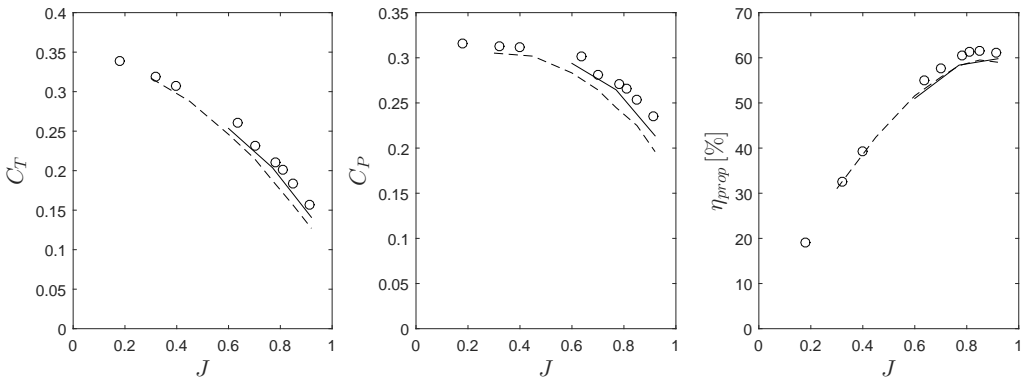


**Figure 6.1.1:** The coefficient of thrust  $C_T$ , coefficient of power  $C_P$ , and propeller efficiency  $\eta_{prop}$  for experiments ( $\circ$ ), CFD ( $- -$ ), and compensated CFD ( $-$ ).



## 6.2 Cruise performance results

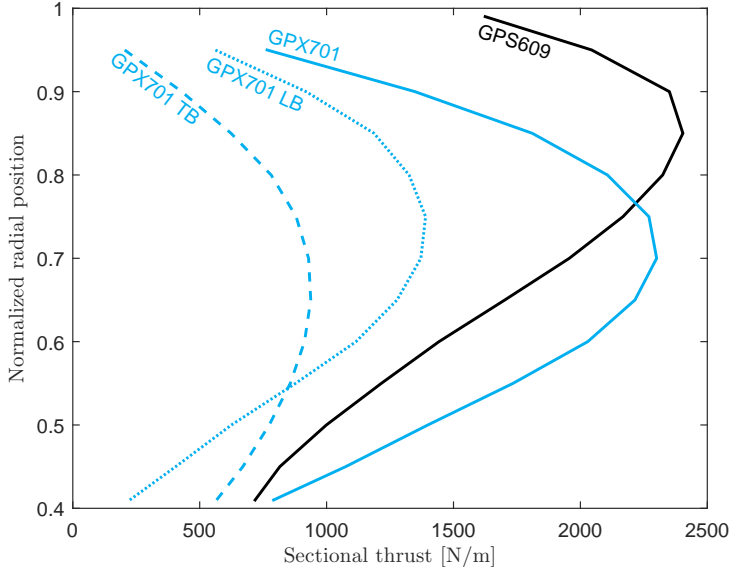


**Figure 6.2.1:** The sectional thrust ( $T'$ ) for the GP-S-609 and the GP-X-701 (Leading (LB) and Trailing Blade (TB)).

The propellers mentioned in Section 4 deliver the following thrust coefficients at cruise:

- **GP-S-609:**  $C_T = 0.4638$
- **GP-X-701:**  $C_T = 0.4640$

Albeit the propellers deliver virtually the same thrust coefficient, they produce the thrust in a slightly different manner, as is illustrated by Figure 6.2.1. The main difference between the analysed propellers is the location of peak sectional thrust  $T' = dT/dr$ , which for the GP-S-609 is closer to the tip region, while for the GP-X-701 it is closer to mid-span. As a consequence, the Boxprop produces more swirl than the conventional propeller. This can be shown analytically by expressing the sectional thrust in terms of the average swirl  $U_\theta$ , which is done by first writing the total circulation  $\Gamma_{wake}$  behind the propeller as a function of the produced swirl:

$$B\Gamma_{wake}(r) = 2\pi r U_\theta \quad (6.2.1)$$

The swirl in the wake can be translated into the amount of sectional lift  $L'$  the propeller blades produce by using the Kutta-Joukowski theorem:

$$\frac{dL}{dr} = L' = B\rho V_{\infty,r} \Gamma_{wake} = 2\pi r \rho V_{\infty,r} U_\theta \quad (6.2.2)$$

The sectional lift can in turn be used to express the sectional thrust produced by the propeller:

$$T' = L' \cos(\phi) - D' \sin(\phi) = L' \cos(\phi)(1 - \epsilon \tan(\phi)) \quad (6.2.3)$$

$$\rightarrow T' = 2\pi r \rho V_{\infty, r} U_{\theta} \cos(\phi)(1 - \epsilon \tan(\phi)) \quad (6.2.4)$$

If the sectional thrust is constant and the radius approaches the hub, the total blade velocity  $V_{\infty, r}$  and trigonometric terms decrease, and therefore Equation 6.2.4 must result in an increased swirl velocity. Similarly, the swirl velocity will decrease for a constant amount of sectional thrust if the radius approaches the tip. This reasoning is always valid for inviscid flow, or for airfoil drag-to-lift ratios below  $\epsilon \approx 0.1$ .

Figure 6.2.1 also shows that the LB is more loaded than the TB, which is due to the low pressure in the area of supersonic flow that is created in the blade passage. This low pressure region is shown in Figure 6.2.2, where the blade sections near the hub ( $\xi = 0.5$ ) operate relatively independently, in contrast with the flow closer to the tip ( $\xi = 0.75$ ). Near the tip, the suction side of the LB extends to the pressure side of the TB, which effectively decreases the amount of thrust the TB can generate. Also visible is a shock extending through the passage, but which is weaker on the pressure side of the TB. The Mach number distribution for the GP-S-609 is shown in Figure 6.2.3, and is included in order to highlight the differences in the flow field between a conventional propeller and the Boxprop. The Mach numbers of the conventional propeller are lower than for the Boxprop, which most likely is due to the highly swept shape of the GP-S-609 and the lack of a choked blade passage.

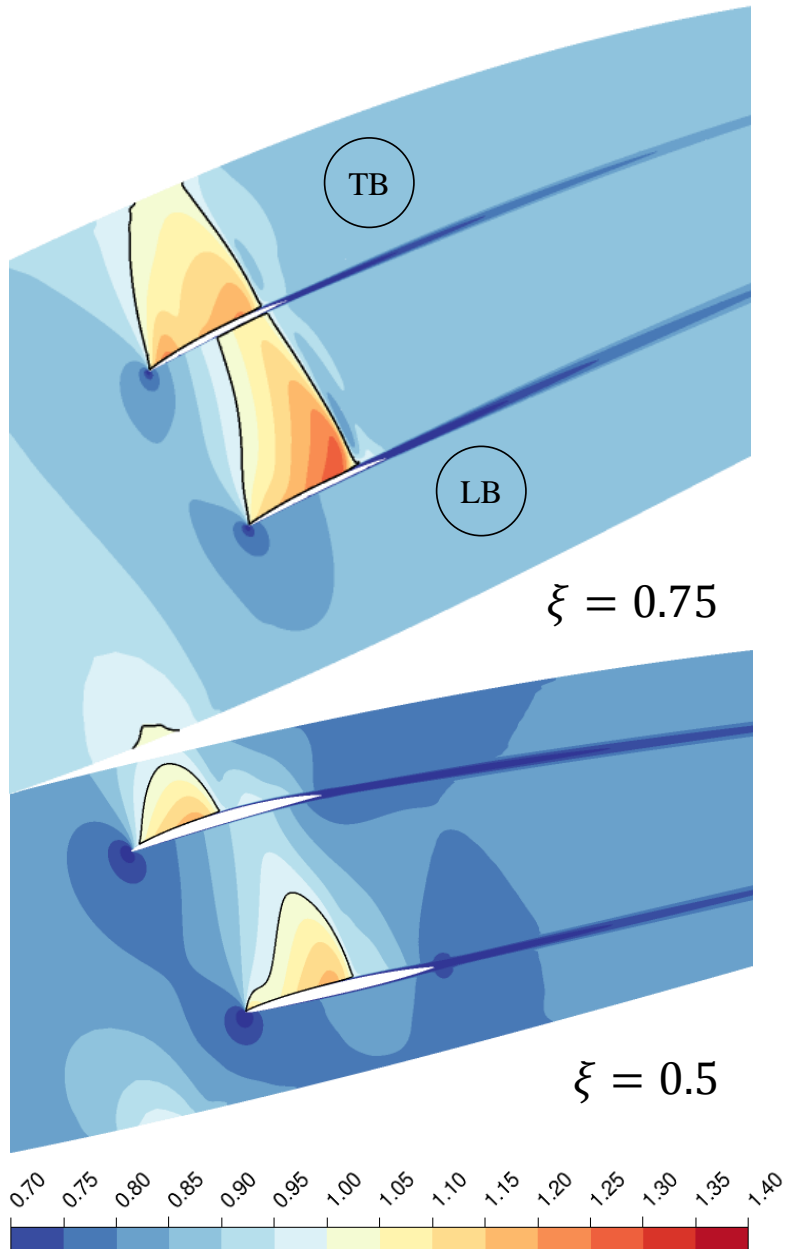


**Figure 6.2.2:** Mach number distribution for the GP-X-701 at non-dimensional radius  $\xi = 0.5$  and  $\xi = 0.75$ . Solid lines denotes Mach 1, which also denotes the location of shocks whenever the upstream flow is supersonic.

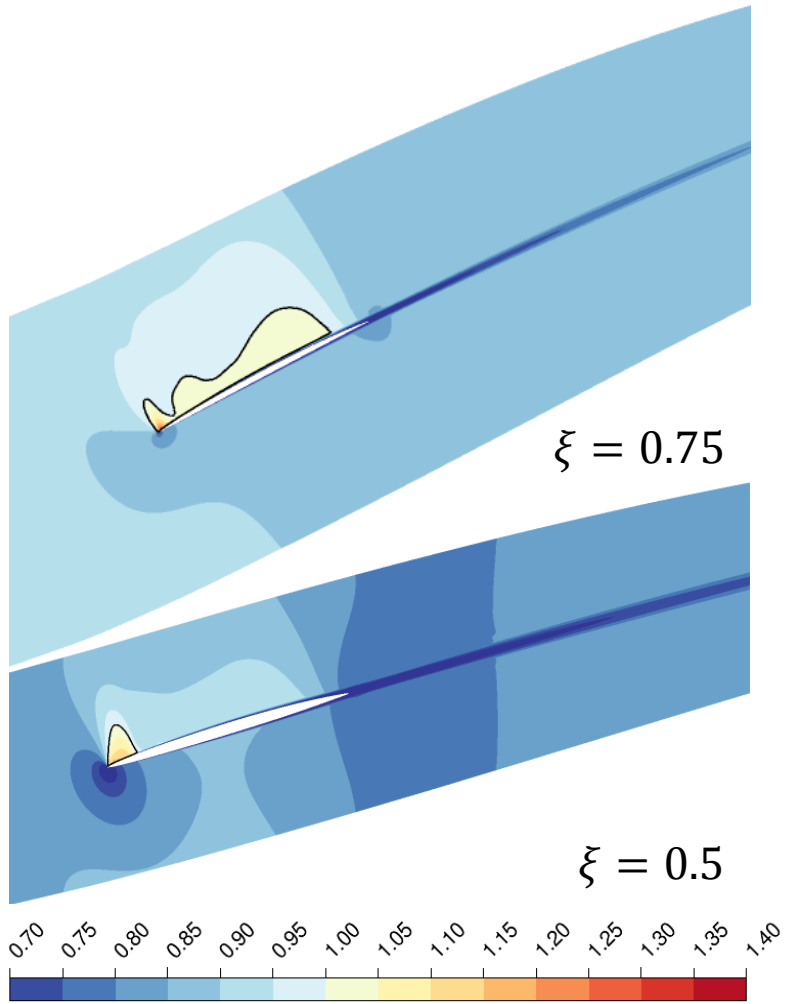


**Figure 6.2.3:** Mach number distribution for the GP-S-609 at non-dimensional radius  $\xi = 0.5$  and  $\xi = 0.75$ . Solid lines denotes Mach 1.

## 6.3 Wake Analysis results

The Wake Analysis Method (WAM) from section 3 has been implemented in MATLAB and was used for analysis of the GP-X-701 and GP-S-609 propellers. The various terms in Eq. 3.1.6 are plotted in Figures 6.3.1 and 6.3.2, and clearly show the presence of the tip vortex on the GP-S-609 propeller, and lack thereof for the GP-X-701. The tip vortex of the GP-S-609 is visible throughout all power flux terms, and show how highly energetic the flow of the tip vortex is compared to the flow around the tip of the Boxprop.

If the power flux terms in Eq. 3.1.6 are integrated on several planes downstream of the propeller and the velocities decomposed into *circumferential averages* and *perturbations*, axial trends are obtained, as have been plotted in Figures 6.3.3 and 6.3.4. The main energy conversion process occurring in both propellers is the transfer of energy between enthalpy and average axial kinetic energy ( $0.5U_x^2$ ), as the increased pressure at the propeller disk accelerates the flow. This behaviour is in accordance with simpler propeller performance models such as the *Actuator Disc Model* or *Blade Element Momentum* theory, where pressure is assumed to be increased discontinuously across the propeller disc, and the flow accelerates downstream. The enthalpy should also increase slightly downstream of the propeller blades due to the dissipation of wakes, boundary layers, tip vortices and mixing, but presently this effect has not been decoupled from the pressure changes.

The averaged swirl ( $0.5U_\theta^2$ ) generated from the propellers stays relatively constant with respect to axial distance, and is about 50% higher for the GP-X-701 than for the GP-S-609. This difference in generated swirl is consistent with the radial position of the peak sectional thrust for the two propellers, as was shown in Figure 6.2.1. The higher amount of swirl would lead to lower efficiency on a single, isolated propeller, but is partially recoverable in a counter-rotating propeller setup.

The kinetic energy of the averaged radial velocity ( $0.5U_r^2$ ) is very low for both propellers, since the majority of this velocity is a velocity perturbation. The perturbation terms account for the amount of kinetic energy bounded to any type of non-uniformity, including wakes and tip vortices. It accounts for around 2.4 – 3.4% of the engine shaft power for the analyzed propellers, and can be considered pure losses. The velocity perturbations are not only losses, but cause noise when they impinge on a rear, counter-rotating propeller, and should therefore be minimized. Alternatively, the rear propeller should be placed sufficiently far downstream for the non-uniformities to mix out. The WAM can both quantify the amount of non-uniformities, and show how they develop downstream of the propeller. As a final note, the perturbation terms are slightly lower for the GP-X-701 than for the GP-S-609 where a rear propeller could be located (0.2 – 0.3D downstream), but are still relatively similar in magnitude. A possible reason for the similar values include the longer blade span of the the GP-X-701, due to the arch shape of the Boxprop concept.

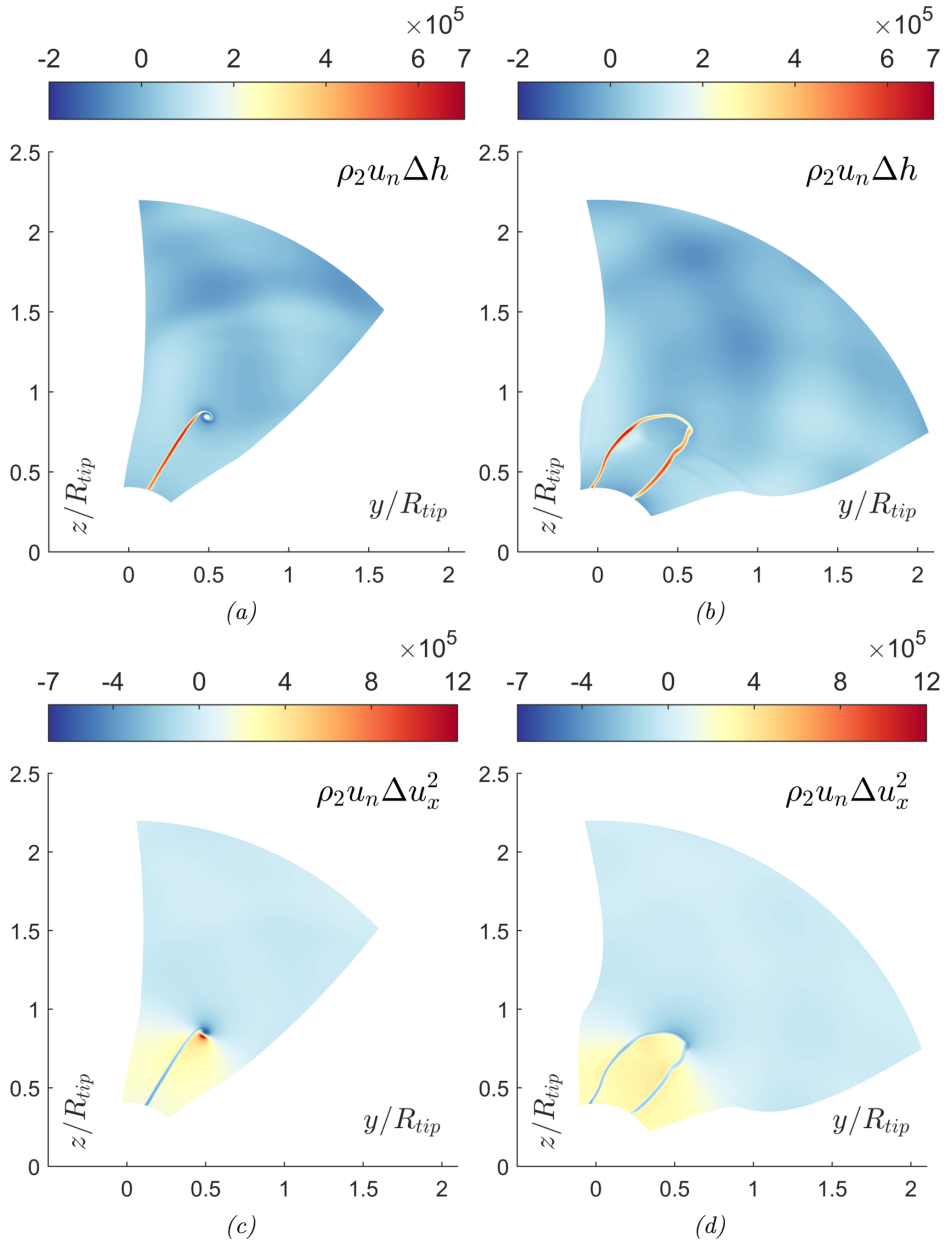


**Figure 6.3.1:** Enthalpy ((a), (b)) and axial kinetic ((c), (d)) power fluxes [ $W/m^2$ ] for the GP-S-609 ((a), (c)) and GP-X-701 ((b), (d)) propellers. The planes are located 0.2D downstream of the propeller trailing edge at 75% radius. The displayed values are multiples of  $10^5 W/m^2$

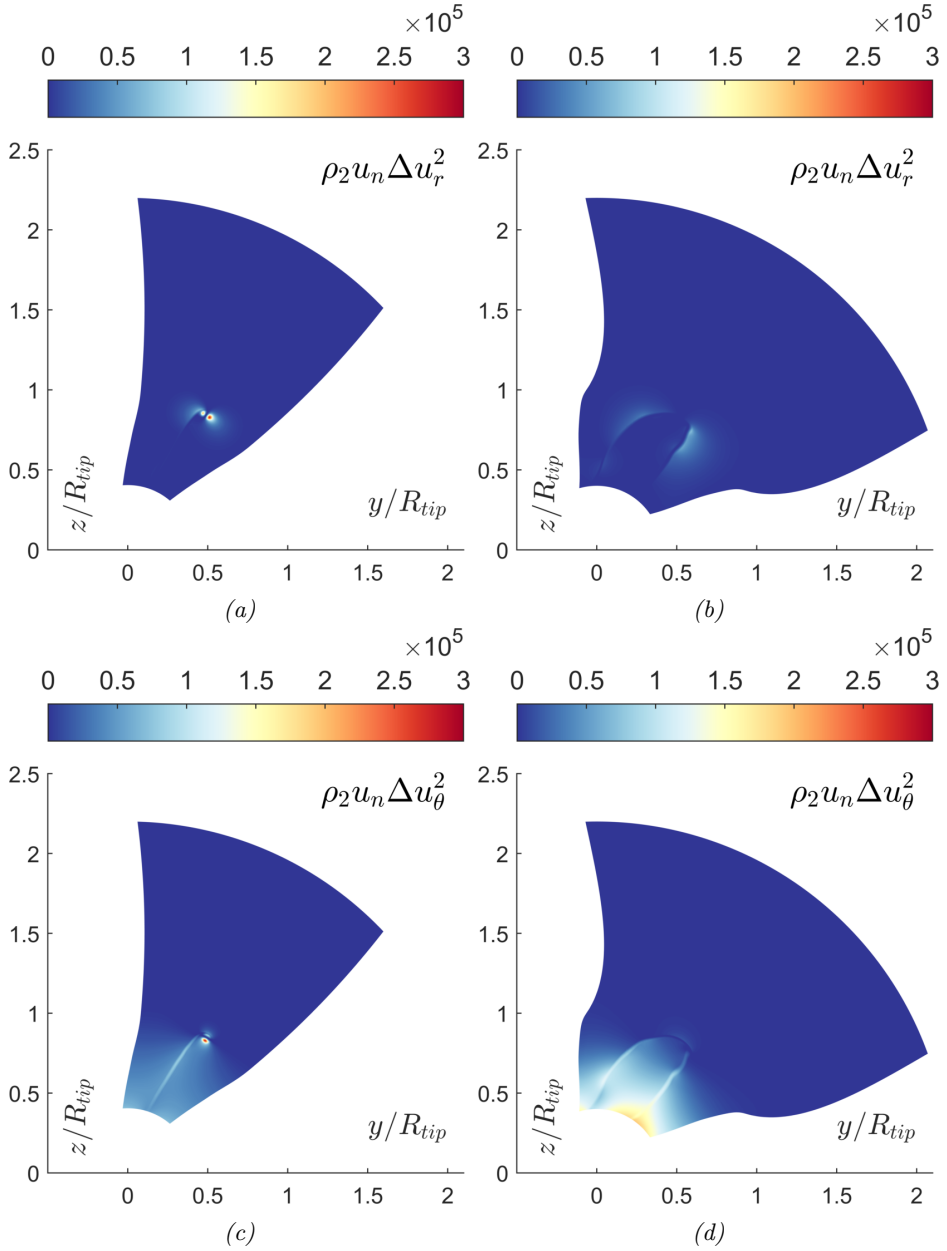


**Figure 6.3.2:** Radial ((a), (b)) and tangential kinetic ((c), (d)) power fluxes [W/m<sup>2</sup>] for the GP-S-609 ((a), (c)) and GP-X-701 ((b), (d)) propellers. The planes are located 0.2D downstream of the propeller trailing edge at 75% radius. The displayed values are multiples of  $10^5$  W/m<sup>2</sup>

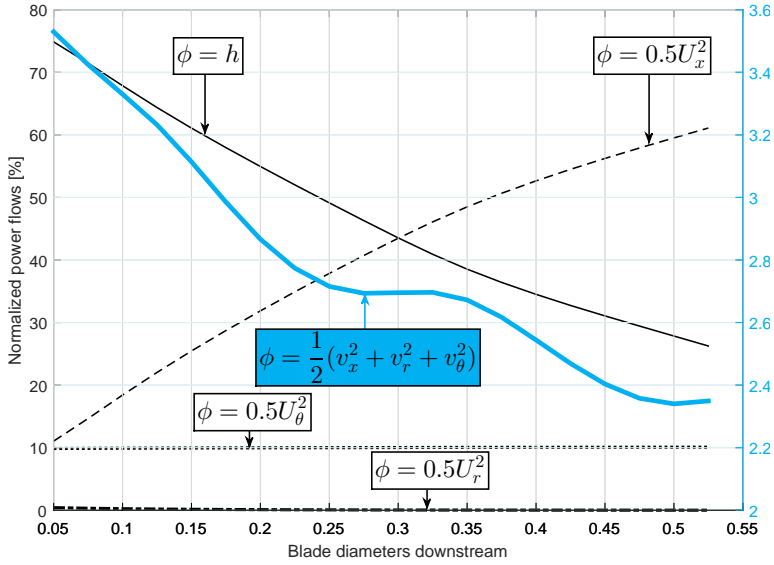


**Figure 6.3.3:** Power integrals  $\int \rho u_n \Delta \phi dA$  normalized by shaft power as a function of axial distance for the GP-S-609 propeller. The kinetic energy bounded to the perturbation velocities are plotted on a separate axis.

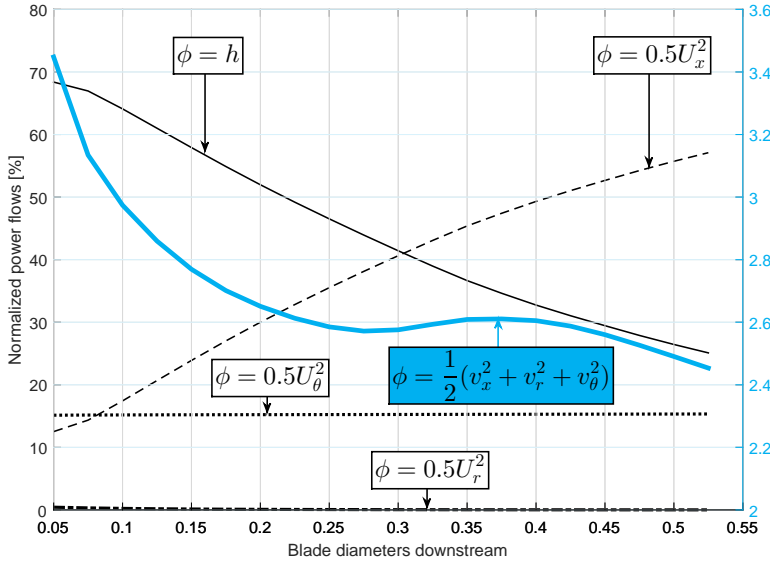


**Figure 6.3.4:** Power integrals  $\int \rho u_n \Delta \phi dA$  normalized by shaft power as a function of axial distance for the GP-X-701 propeller. The kinetic energy bounded to the perturbation velocities are plotted on a separate axis.



## 6.4 Boxprop tip flow

One of the main hypotheses of the Boxprop is that the tip vortex can be eliminated, and this has been shown to be true for the GP-X-701 propeller. As expected, in Figure 6.4.1 the vorticity magnitude and intertwined streamlines show the presence of a tip vortex on the GP-S-609, and lack thereof on the GP-X-701.

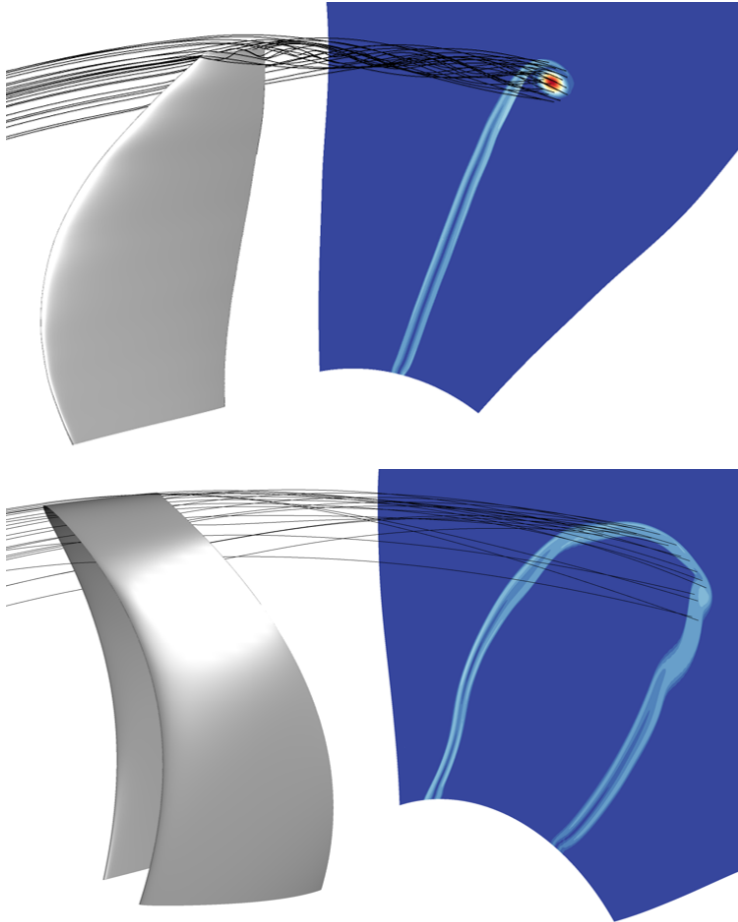


**Figure 6.4.1:** Streamline plots of the flow around the blade tips for the GP-S-609 (left) and the GP-X-701 propellers (right). The planes display the vorticity  $0.2D$  downstream of the propeller blade trailing edge, and use identical color scaling.

# 7 Conclusions

## 7.1 Meshing

The following conclusions have been drawn during the work leading up to the publications included in this thesis:

- **Tetrahedral meshing** is sufficient for estimating performance using CFD, but there are a number of factors to take into consideration, namely computational effort and un-physical dissipation. *The computational effort* stems from the necessity of properly resolving the sharp geometric features found in propeller blades, and the fact that tetrahedral elements should be isotropic in size to maintain a relatively high quality. These two issues lead to tetrahedral meshes with very large amounts of cells. *The un-physical dissipation* has its origin in that a tetrahedral mesh is usually not aligned with the flow direction. Additionally, controlling refinement in specific directions produces elements with bad quality, which in the end can lead to sharp features such as wakes to be "washed out" in the computational domain. These issues *can* generally be overcome with tetrahedral meshes, but only with an enormous amount of cells. All these factors together make tetrahedral meshes unsuitable for the purpose of using them in the Wake Analysis Method.
- **Hexahedral meshing** results in meshes with lower cell counts, lower un-physical dissipation and higher refinement control. The main disadvantage in applying this meshing approach on a Boxprop is the complex blade shape and resulting blocking structure. The meshing complexity is considerably higher than for a conventional propeller, necessitating more support geometry, and longer setup times. The main benefit of using hexahedral meshes for the Wake Analysis Method is the ability to refine the mesh in the direction normal to the flow, which prevents un-physical dissipation of the perturbation terms in the analysis method.

## 7.2 Performance and modelling

- The latest Boxprop geometry designed for cruise conditions can deliver a **thrust comparable** to published CROR front rotors, albeit with higher amounts of swirl, which can be recoverable in a rear counter-rotating propeller.
- The **WAM** is capable of quantifying the losses in wake flow structures and relate them directly to engine power. Any type of axial turbomachine could potentially be analysed with the same methodology, and its losses quantified and compared between different designs.
- **No tip vortex** has thus far been observed on the Boxprop. When simulating future designs, operating points, and power levels, the presence/lack of the tip vortex needs to be verified.

## 8 Future work

A number of initiatives are ongoing or planned for the near future based on the lessons learned from the work presented in this thesis:

- Aerodynamic optimization of the Boxprop - The work this far has shown that the current Boxprop designs produce more swirl than conventional propellers, which has a negative effect on efficiency. This can be remedied by shifting the peak sectional thrust closer to the blade tip. This shift is challenging due to the complex shape of the Boxprop and transonic flow regime. Considering this and the existing experience in the Division with regards to stochastic optimization, a future goal should be to optimize the Boxprop geometry using a meta-model assisted multi-objective Genetic Algorithm. The end result should be a database of various optimal propeller designs with respect to thrust and efficiency.
- Rear rotor for CROR - A conventional propeller should be designed for use in a CROR setup, downstream of a Boxprop. Design software for conventional propellers has already been developed, and the remaining work should focus on automating geometry and mesh creation.
- CROR nacelle design generation - A nacelle geometry should in the future be parametrized and optimized with regards to nacelle drag and minimizing Mach number at the front propeller disc.
- CROR Performance simulation with Boxprop - A complete CROR employing a Boxprop as the front rotor, conventional propeller as rear rotor, and optimized nacelle should be simulated with CFD. This work could serve as stepping stone for estimating the noise signature of a Boxprop in a CROR.

# 9 Summary of Papers

## 9.1 Paper I

R. Avellán, A. Capitao Patrao, A. Lundbladh, and T. Grönstedt, 2015, Preparing for Proof-of-Concept of a Novel Propeller for Open Rotor Engines, *22nd ISABE Conference*, October 25–30, Phoenix, USA.

### 9.1.1 Division of work

In this paper I supervised the experimental and computational work which compared the performance obtained with CFD and the Chalmers Wind Tunnel. I also performed the design, meshing, and simulation of the GP-X-701 propeller at cruise conditions and developed the Wake Analysis Method together with Anders Lundbladh. My co-authors contributed with insights and analysis of the obtained numerical and experimental results. Richard Avellán was the main author of the paper, and coordinated the work on material selection, manufacturing processes, and pitch mechanisms for small scale propellers.

### 9.1.2 Summary

This paper summarizes the development of the Boxprop during the period between 2013 and 2015. Progress on small scale testing with 3D printed plastic propellers are reported and compared to CFD results for near take-off conditions. Very good agreement is obtained in terms of performance values for experiments and CFD.

New insights gained from a student project on the manufacturing of metallic small scale propellers is presented. The choice of manufacturing process (multi-axis milling, Electron Beam Melting (EBM), and Selective Laser Melting (SLM)) and its effect on cost, surface finish, and lead times is presented. The milled blades had excellent surface finish, but longer lead times and five times higher cost than an entire 3D-printed plastic propeller. The blades manufactured with additive methods (EBM and SLM) had lower lead times and were cheaper than the milled blade, but unfortunately possessed a much higher surface roughness, thus requiring polishing after-treatments.

The development of Boxprop design for cruise is presented in terms of efficiency and thrust. These two performance parameters have increased substantially since the start of the research project, and the underlying flow features and geometric changes that have lead to these increases in performance are presented. The two main design changes is the tailoring of the tip of the Boxprop to the oncoming flow, and the use of different camber and angle-of-attack for the two blade halves, which decreases blade interference in the blade passage.

The Wake Analysis Method was initially presented and derived in this paper. The velocity was shown be decomposable into a circumferential average and an associated perturbation, of which the latter accounts for velocities in tip vortices and wakes behind a propeller. Very brief results from this theory were presented for a conventional propeller inspired by the NASA SR7L propeller.

## 9.2 Paper II

A. Capitao Patrao, R. Avellán, A. Lundbladh, and T. Grönstedt, 2016, Wake and Loss Analysis for a Double Bladed Swept Propeller, *Proceedings of ASME Turbo Expo 2016*, June 13–17, Seoul, South Korea.

### 9.2.1 Division of work

Besides being first author, my contribution was designing both the conventional propeller and the Boxprop, performing their meshing, and simulation. Additionally, I developed procedures and scripts for sampling data in the CFD results for the WAM. A lot of time and effort went into finding the right mesh for this method, particularly in terms of mesh convergence. My co-authors supervised my work and aided in the analysis of the results. My co-authors also contributed with large parts of the introduction, discussion, and conclusions.

### 9.2.2 Summary

The main aim of this paper was to highlight the differences in the wake between a conventional propeller and the Boxprop, and use this information as guidance for future, improved designs. The geometries of the conventional propeller GP-S-609 and the Boxprop GP-X-701 are described in relatively high detail, as is the adopted computational method.

Performance-wise, the GP-X-701 Boxprop can provide the necessary thrust to replace the front rotor of modern, published CROR designs. The major caveat is the higher amount of swirl compared to the GP-S-609 propeller, which is evident both in the location of the peak sectional thrust and in the WAM results. This higher amount of swirl can be partially recovered in the rear, counter-rotating propeller of a CROR. The major reason that this particular Boxprop design is loaded closer to the hub is the blade interference in the blade passage. This blade interference prevents the trailing blade from producing any large amount of thrust in the vicinity of the blade tip, therefore requiring more thrust to be produced closer to the hub, which results in more swirl.

In this paper the WAM shows clearly the main energy transfer process occurring downstream of the propeller, specifically between static pressure and axial kinetic energy, which is in accordance to existing propeller models such as the Actuator Disc Model. Furthermore, the method has been used to quantify the fraction of engine power that has been transferred to the kinetic energy of swirl (which is recoverable) and to the wakes and tip vortices (which is not recoverable). The kinetic energy of the perturbations as a fraction of engine power is shown to be similar in magnitude for both propellers, but is slightly lower for the Boxprop where a possible rear rotor would be located. This might give some initial insight into how the Boxprop will perform from an acoustic point-of-view. Lower perturbation energies indicate weaker flow perturbations, which might result in lower amounts of noise when these flow perturbations impinge on a rear, counter-rotating propeller.



# Bibliography

- [1] Axelsson, A., Göransson, A., Hung, C., Klipic, S., Landahl, J., Olofsson, J., Thor, D., 2012. Development of a Box-Bladed Propeller - Mechanical Analysis and Feasibility Study of the Concept. Tech. rep., Chalmers University of Technology, Department of Product Development. Part of the project course MPP126.
- [2] IATA Air Passenger Forecast Shows Dip in Long-Term Demand. <http://www.iata.org/pressroom/pr/Pages/2015-11-26-01.aspx>. Accessed: 2016-05-16.
- [3] IATA Annual Review 2015. <https://www.iata.org/about/Documents/iata-annual-review-2015.pdf>. Accessed: 2016-05-16.
- [4] Nitrogen Dioxide - Health. <https://www3.epa.gov/airquality/nitrogenoxides/health.html>. Accessed: 2016-05-16.
- [5] Thulin, O., 2016. On Exergy and Aero Engine Applications.
- [6] Beauty of Future Airplanes is More than Skin Deep. [https://www.nasa.gov/topics/aeronautics/features/future\\_airplanes.html](https://www.nasa.gov/topics/aeronautics/features/future_airplanes.html). Accessed: 2016-09-05.
- [7] Negulescu, C. A., 2013. “Airbus AI-PX7 CROR Design Features and Aerodynamics”. *SAE International Journal of Aerospace*, **Vol. 6**(Issue: 2), pp. 626–642.
- [8] van Zante, D., 2015. “Progress in Open Rotor Research: A U.S. Perspective”. In Proceedings of ASME Turbo Expo 2015, no. GT2015-42203.
- [9] Schnell, R., Yin, J., Voss, C., and Nicke, E., 2012. “Assessment and Optimization of the Aerodynamic and Acoustic Characteristics of a Counter Rotating Open Rotor”. *Journal of Turbomachinery*, **Vol. 134**(Issue: 6), p. 61016.
- [10] Vlastuin J., Dejeu C., L. A., and J., T., 2015. “Open Rotor Design Strategy from Wind Tunnel Tests to Full Scale Multi-Disciplinary Design”. In Proceedings of ASME Turbo Expo 2015, no. GT2015-43300.
- [11] Airbus, Snecma Tackle Open-Rotor Integration. <http://aviationweek.com/equipment-technology/airbus-snecma-tackle-open-rotor-integration>. Accessed: 2016-05-16.
- [12] Kroo I., 2005. “Nonplanar Wing Concepts for Increased Aircraft Efficiency”. In VKI lecture series on Innovative Configurations and Advanced Concepts for Future Civil Aircraft.
- [13] Avellán, R. and Lundbladh. Air Propeller Arrangement and Aircraft. International Patent Application WO2011/081577A1, filed on Dec 28, 2009.
- [14] Adriansson S., 2013. “Design and testing of a box-bladed propeller”. Master’s thesis, Chalmers University of Technology.

- [15] Lindsey WF and Stevenson DB, 1948. "Aerodynamics Characteristics of 24 NACA 16-Series Airfoils at Mach Numbers Between 0.3 and 0.8".
- [16] Olofsson, J., and Petterson, V., 2013. "Experimental investigation of an innovative high speed propeller". Master's thesis, Chalmers University of Technology.
- [17] A., S., and J., Y., 2009. "Low-Speed Aerodynamics and Aeroacoustics of CROR Propulsion Systems". American Institute of Aeronautics and Astronautics.
- [18] Violette, J.A., Sullivan, W.E., and Turnberg, J.E., 1984. Large-Scale Advanced Prop-Fan (LAP) blade design. Tech. rep., Hamilton Standard, Windsor Locks, CT, United States. Paper No. NACA-CR-174790.
- [19] ANSYS CFX Solver Modelling Guide 14.5, ANSYS Inc. 2014.
- [20] Lind A., 2013. "Aerodynamic Simulations of an Innovative High Speed Propeller". Master's thesis, Chalmers University of Technology.
- [21] Busch, S. and Jonsson, I., 2015. "Wind Tunnel Test of a Double Blade Swept Propeller and Analysis of Real Geometry Effects". Master's thesis, Chalmers University of Technology.